

Primljen / Received: 13.11.2019.

Ispravljen / Corrected: 23.1.2020.

Prihvaćen / Accepted: 15.3.2020.

Dostupno online / Available online: 10.12.2020.

Comparative analysis of tripod offshore structure

Authors:



Assoc.Prof. **Engin Gücüyen**, PhD. CE
Manisa Celal Bayar University, Turkey
Faculty of Engineering
Department of Civil Engineering
engin.gucuyen@cbu.edu.tr



M. Ensar Yiğit, PhD. CE
Manisa Celal Bayar University, Turkey
Faculty of Engineering
Department of Civil Engineering
ensar.yigit@cbu.edu.tr



Assoc.Prof. **R. Tuğrul Erdem**, PhD. CE
Manisa Celal Bayar University, Turkey
Faculty of Engineering
Department of Civil Engineering
tugrul.erdem@cbu.edu.tr
Corresponding author



Prof. **Ümit Gökkuş**, PhD. CE
Manisa Celal Bayar University, Turkey
Faculty of Engineering
Department of Civil Engineering
umit.gokkus@cbu.edu.tr

Professional paper

Engin Gücüyen, M. Ensar Yiğit, R. Tuğrul Erdem, Ümit Gökkuş

Comparative analysis of tripod offshore structure

Marine structures are nowadays used in a variety of ways. The analysis of a tripod-type offshore structure sixty m in total height is performed in this study. In addition to operation-related loads, the structure is also under the effect of wind and wave loads. While the Eurocode velocity profile is used to calculate wind forces, the Airy wave velocity profile is utilized to determine wave forces. The model is created by a finite elements analysis program, and is composed of fluid and structural parts. The interaction of the parts is ensured by Coupled Eulerian Lagrangian (CEL) technique.

Key words:

offshore structures, fluid-structure interaction, finite element analysis, Coupled Eulerian Lagrangian technique

Stručni rad

Engin Gücüyen, M. Ensar Yiğit, R. Tuğrul Erdem, Ümit Gökkuş

Usporedna analiza tronožne odobalne građevine

Pomorske se konstrukcije u današnje vrijeme koriste za razne namjene. U ovom se radu analizira odobalna građevina tronožnog tipa ukupne visine šezdeset metara. Uz opterećenja vezana za samo funkcioniranje, konstrukcija građevine podvrgnuta je i opterećenjima uslijed djelovanja vjetera i valova. Za proračun sile vjetera korišten je profil brzine prema europskoj normi, a za određivanje sile valova Airyeva brzina valova. Model je izrađen pomoću programa za analizu konačnih elemenata, a sastoji se od fluidnog i konstrukcijskog dijela. Interakcija između tih dijelova postignuta je kombiniranim Euler-Lagrangeovim postupkom (CEL).

Ključne riječi:

odobalne građevine, interakcija fluida i konstrukcije, analiza konačnih elemenata, kombinirani Euler-Lagrangeov postupak

Fachbericht

Engin Gücüyen, M. Ensar Yiğit, R. Tuğrul Erdem, Ümit Gökkuş

Vergleichende Analyse einer dreibeinigen Offshore-Struktur

Maritime Strukturen werden heutzutage für verschiedene Zwecke genutzt. In dieser Arbeit wird eine dreibeinige Offshore-Struktur mit einer Gesamthöhe von 60 Metern analysiert. Zusätzlich zu den Belastungen, die sich auf die Funktionsweise selbst beziehen, ist die Struktur des Gebäudes auch Belastungen aufgrund der Einwirkung von Wind und Wellen ausgesetzt. Das Geschwindigkeitsprofil gemäß der europäischen Norm wurde verwendet, um die Windkraft zu berechnen, und die Wellengeschwindigkeit nach Airy wurde verwendet, um die Wellenkraft zu bestimmen. Das Modell wurde mit einem Finite-Elemente-Analyseprogramm erstellt und besteht aus einem Fluid- und einem Strukturteil. Die Wechselwirkung zwischen diesen Teilen wurde durch das kombinierte Euler-Lagrange-Verfahren (CEL) erreicht.

Schlüsselwörter:

Offshore-Strukturen, Fluid-Struktur-Wechselwirkung, Finite-Elemente-Analyse, kombiniertes Euler-Lagrange-Verfahren

1. Introduction

Energy requirement increases with an increase in the world's population. Energy supply and storage facilities in the open seas develop due to depletion of fossil fuels on land and increase in the cost of land. Structures in open seas, where clean energy sources such as wave and wind are produced, have become significant construction sites. Offshore structures are also used for air and sea transportation.

The practice of building wind turbines on offshore structures has been rapidly increasing in recent times. These structures provide services as floating structures or as structures that are anchored to sea bottom. From the point of view of engineering design, many difficulties are encountered in the case of floating turbines such as more advanced blade control because of the floating motion, heavy loads on the tower, and the complexity and high cost of installation operations [1]. While substructure and foundation parts are cheaper, the turbine is more expensive for bottom-fixed offshore wind platforms. On the other hand, substructure and foundation parts are more expensive for floating offshore wind platforms. Thus, the overall cost difference between fixed-bottom and floating offshore wind applications is high [2]. There are also several difficulties with regard to the design, production, installation, control, and operation phases of the floating offshore wind turbines. Floating structures are susceptible to some negative occurrences such as fracturing, entrainment and submersion. The mooring system is significant in terms of the station-keeping of floating offshore wind turbines in marine environment [3]. The industry is burdened with the lack of experience because of the limited number of installations and the differences in platform design [4].

Offshore fixed platforms can be classified as gravity, monopile, tripod, and jacket platforms [5]. Tripod foundations involve three medium diameter steel pipe piles configured in an equilateral triangle, whose apex supports the upper tripod part of the truss structure. Tripod truss manufactured as a precast part may resist bigger loads that affect the tower, and transfer stresses to three steel piles.

In addition to wave forces, wind, flow, ice and earthquake forces may also effect tripod type offshore structures as environmental loads [6]. The design is only performed according to wave loads for massive wave loads and wave run-up situations [7, 8]. KDue to an increase in height of the structure above water level, the combination of wind and wave loads can be experienced [9]. Since wave forces are unstable and more destructive than wind forces, they are more determinant in dynamic analysis [10]. Diffraction Theory [11] or Morrison Equation [12] is used to calculate the wave force.

One of the methods used to determine dynamic behaviour of offshore structures is the fluid-structure interaction analysis. The analysis type is unidirectional when force is transferred from fluid to structure only. On the other hand, when force is transferred from fluid and displacement is transferred from structure, the analysis type is bidirectional. Finite element

method is the most common one for both types of analysis. Finite element supported fluid-structure interaction analyses can be performed by Eulerian method alone [13], Lagrange method alone [14] or Arbitrary Lagrangian Eulerian (ALE) [15, 16] and Coupled Eulerian Lagrangian (CEL) [17, 18] methods in which both methods are utilized. The Abaqus software is commonly used for interaction modelling operations [19]. While the structure is modelled as Lagrangian part, fluid is modelled as Eulerian part in ALE and CEL analyses. Because the interaction surface and co-simulation are not defined, these methods present advantages over methods that are only Lagrangian or Eulerian. In addition, high structural element distortions that occur in ALE method may cause inappropriate results in the software [20]. CEL method which is a large deformation finite element analysis, removes the disadvantages of pure Lagrangian and Eulerian methods in the software by utilizing an explicit time integration scheme [19]. CEL is formed from Eulerian mesh that shows the volume where the Eulerian material flows and interacts with Lagrangian part. By using the traditional Eulerian description/mesh in which the numerical grid is fixed in space when water flows through the grid, fluid motion in CEL can be defined. On the other hand, inflatable structure is defined when the numerical grids move and deform with the material in the traditional Lagrangian description of motion in the Lagrange method [18, 21].

According to relevant literature, analytical [22], numerical [23] and experimental methods [24] have been used to model dynamic behaviour of the pile-supported offshore structures. In this study, the dynamic behaviour of structures under the effect of wind and wave forces is investigated by semi-analytical and numerical methods. While the semi-analytical method includes the unidirectional fluid-structure interaction, the numerical analysis involves bidirectional interaction. The CEL approach is used in the Abaqus software in the numerical method. While the structure is modelled by Lagrangian method, marine environment around the structure is modelled by Eulerian method. Afterwards, the structure is modelled as a two-degree of freedom system by lumped masses. The displacement and natural frequency values are obtained by numerically solving the equation of motion of a two degree of freedom system using the Runge-Kutta method. Thus, differences between numerical and semi analytical models are determined in terms of displacements and natural frequencies.

2. Template structure and environment

Numerical and semi-analytical models of the structure are presented in Figure 1. Besides, the structure constituting the Lagrangian model and CEL model of the marine environment that forms the Eulerian model is shown in Figure 1. While the upper part of the structure consists of wing, tribune and column carrying the generator, the bottom part of the structure is formed of three steel piles carrying the upper part. The piles are connected to each other by vertical and diagonal members.

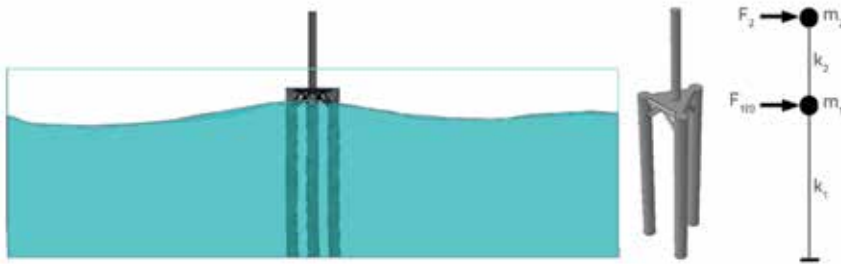


Figure 1. Numerical and semi-analytical models

The height of the substructure and the upper structure is 40 m and 20 m, respectively. Thus, the total height of the structure is 60 m. The diameter of steel piles that constitute the legs of the substructure is 1.50 m, and the wall thickness is 0.01 m. Steel bracing members are 0.50 m in diameter and 0.005 m in wall thickness. Thirty-five meters of the substructure are in the contact with the sea, and the remaining 5 meters are in the contact with air. The steel column that generates the upper structure is 1.50 m in diameter and 0.005 m in wall thickness. The column centre-to-centre spacing (b) is 10 meters. Total weight of the wing, turbine and generator is 4.00×10^5 kg modelled as lumped mass and placed on the peak point of the column.

Marine environment of the structure is modelled with wave and wind forces. Velocity profile of the linear wave theory is used to model wave, the Eurocode velocity profile is utilized to model wind. Velocity profile of the linear wave theory (u) is given in Equation (1).

$$u = \frac{H}{2} \frac{gT}{L_w} \frac{\cosh[2\pi(y+d)/L_w]}{\cosh(2\pi d/L_w)} \cos\left(\frac{2\pi}{L_w}x - \frac{2\pi}{T}t\right) \quad (1)$$

H is the wave height, T is the wave period, g is the gravity, L_w is the wave length, d is the water depth, t is the time, x and y represent horizontal and vertical positions in the equation. In this paper, marine environment is provided by considering $d = 35$ m, $T = 6$ s and $H = 4$ m. The wave length (L_w) is computed as 56.20 m according to these values. Equation (1) is used for inlet velocity equation of wave in numerical analysis. On the other hand, Equation (1) and Equation (2) are utilized to calculate wave forces in the semi analytical analysis. Wave acceleration (\dot{u}) is determined in Eq. (2).

$$\dot{u} = \frac{g\pi H}{L_w} \frac{\cosh(2\pi(y+d)/L_w)}{\cosh(2\pi d/L_w)} \sin\left(\frac{2\pi}{L_w}x - \frac{2\pi}{T}t\right) \quad (2)$$

The Morison equation Equation (3) is used to calculate wave forces affecting the structure. According to the equation, the total horizontal wave force (F_1) is calculated as the sum of drag (F_D) and inertia (F_I) forces.

$$F_1 = F_D + F_I = \int_{-d}^{\eta} \frac{1}{2} \rho_w C_D D u(y,t) |u(y,t)| dy + \int_{-d}^{\eta} \rho_w C_M \frac{\pi D^2}{4} \dot{u}(y,t) dy \quad (3)$$

In the above equation, ρ_w represents the density of salty water, D is the diameter and η is the distance of the free surface to the still water level. C_D and C_M are drag and inertia coefficients whose numerical values are $C_D = 0.7$ and $C_M = 2.0$, respectively. Wave force that is obtained by Equation (3) is the time varying external force that is used for the unidirectional fluid-structure interaction analysis. In addition, the other external

force is the time independent wind force. The Eurocode velocity profile (u_a) that is utilized to model wind is given in Equation (4) [25].

$$u_a = U_{BAS} k_t \ln(y/z_0) \quad (4)$$

U_{BAS} represents the wind velocity (24 m/s), k_t is the terrain factor (0.17) and z_0 represents the roughness length (0.01) in Equation (4). The relationship between the wind velocity and the wind load on an object is given in Equation (5).

$$F_2 = \int_{\eta}^{L-\eta} \frac{1}{2} \rho_a u_a^2(y) C_s A(y) dy \quad (5)$$

In Equation (5), A is the cross sectional area of the element, ρ_a is the density of the air and C_s represents the shape coefficient which is 0.50 for cylindrical elements and 2.0 for rectangular elements [25]. Wind force, which is determined by Equation (5), is effected to the peak point of the superstructure in both analyses.

3. Analyses

The analyses are performed in two main sections, i.e. the coupled Eulerian Lagrangian (CEL) analysis and the semi-analytical analysis.

3.1. Coupled Eulerian Lagrangian (CEL) analysis

Fluid-structure interaction analyses are widely performed to determine behaviour of offshore structures under environmental loads. The finite elements analysis method is the most commonly used for these analyses. In the numerical part of this study, the fluid-structure interaction analysis is performed by the Abaqus finite elements analysis software. In the finite element analysis, the structure is modelled by Lagrange approach, and the fluid is modelled by Eulerian approach. The analysis is performed using the CEL technique. In the finite element analysis, the software utilizes a combination of Eulerian-Lagrangian approaches, which is the (CEL) method, using equations that are given below. Eqs. (6-8) are the mass, momentum and conversion of energy equations, respectively.

$$\frac{D\rho}{Dt} + \rho \nabla \cdot v = 0 \tag{6}$$

$$\rho \frac{Dv}{Dt} = \nabla \cdot \sigma + \rho b \tag{7}$$

$$\frac{DE}{Dt} = \nabla \cdot (\sigma \cdot v) + \rho b \cdot v \tag{8}$$

where:

- v - velocity,
- ρ - density,
- σ - the Cauchy stress,
- b - the body force,
- E - the total energy per unit volume.

Equations of Lagrangian conservation are converted to the equations of Eulerian conservation according to Equation (9). Equations of Eulerian governing have the general conservation form that is presented in Equation (10). On the other hand, ϕ is a randomly selected solution variable.

$$\frac{D\phi}{Dt} = \frac{\partial \phi}{\partial t} + v \cdot (\nabla \phi) \tag{9}$$

$$\frac{\partial \phi}{\partial t} + \nabla \cdot \Phi = S \tag{10}$$

In Equation (10), Φ is the flux function, and S is the source term. This equation can be given as two separate equations, as shown in Equations (11) and (12):

$$\frac{\partial \phi}{\partial t} = S \tag{11}$$

$$\frac{\partial \phi}{\partial t} + \nabla \cdot \Phi = 0 \tag{12}$$

When the spatial time derivative is replaced by the material time derivative on the fixed mesh, Equation (11) becomes the same with the standard Lagrangian formulation. The deformed

mesh is moved to the original fixed mesh, and volume of material transported between adjacent elements needs to be calculated for the solutions of Equation (12). Parameters such as the mass, energy, momentum, and stress for Lagrangian solution are explained for the flow of the material between adjacent elements through transport algorithms. In addition to this explanation, more information about CEL formulation can be found in [26, 27].

The CEL technique is an effective method for fluid-structure interaction problems, including extreme deformation and fluid flow. The interaction between the two domains has been discretized using the general contact algorithm based on the penalty contact method. Mesh distortion problems involving Lagrangian and Eulerian phases in time increments are easily approached using the CEL method. The nodes are supposed to be fixed with the material as temporary, and the elements deform with the material in the Lagrangian phase. A tolerance is used to specify the elements that are highly deformed after the Lagrangian phase. On the other hand, the deformation is suspended and the elements having remarkable deformation are re-meshed in the Eulerian phase [19, 28].

3.1.1. CEL Application to template structure

The bidirectional fluid structure interaction analysis is performed in this study using the CEL method. The Eulerian part is formed of material assigned and unassigned (void) parts. Dimensions, boundary conditions, and mesh structure of the finite elements model, are shown in Figure 2. The numerical model has 30 x 170 m base dimensions. Its height is 37 m. While width of the finite elements model is determined as three times of the distance between columns (3 x b), the length of the model is taken as being equal to three wave lengths (3 x Lw). In addition, the height value is the sum of water depth (d) and half of the wave height (H/2). Multiple materials involving voids in an element are supported by CEL method. The Eulerian Volume Fractions (EVF), representing the ratio by way of the material filled with Eulerian elements, are used to track the flowing material in a mesh. When an element is filled by a material, the EVF is equal to 1. However, the EVF is 0 when there is no material in an element.

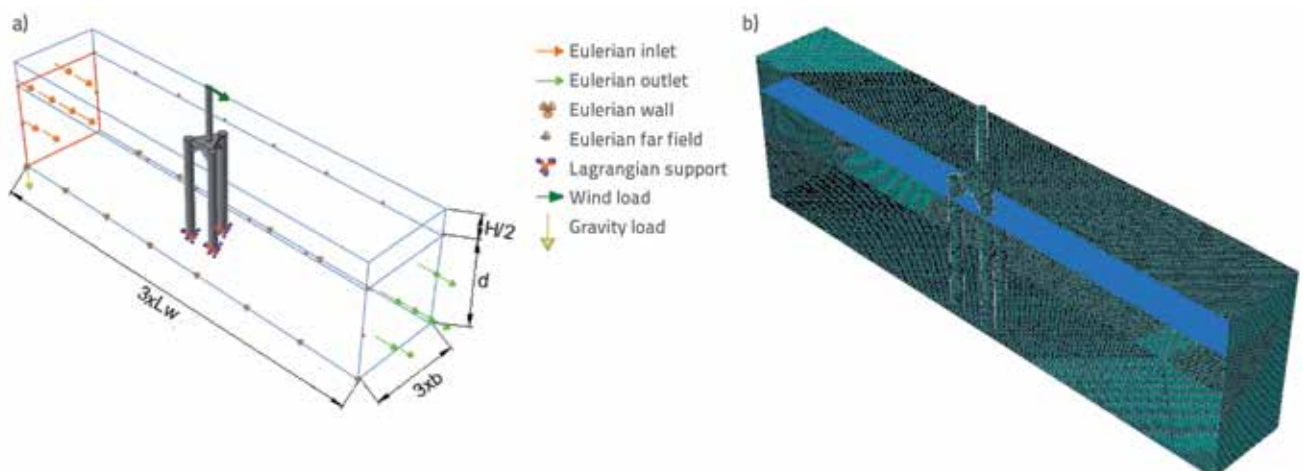


Figure 2. a) Boundary conditions and dimensions; b) Mesh configuration

After the Eulerian and Lagrangian parts are constituted, related materials are assigned to the parts. While characteristics of steel material are used in structural model, characteristics of sea water are used while modelling the marine environment. The sea water is defined as an EOS material in the software. Material properties used in the finite element model are given in Table 1.

Table 1. Material properties of Eulerian and Lagrangian parts

Lagrangian property (steel)		Eulerian property (salty water)	
Density [kg/m ³]	7850	Density [kg/m ³]	1025
Young's modulus [N/m ²]	2.1 × 10 ¹¹	Dynamic viscosity [Ns/m ²]	1.50 × 10 ⁻³
Poisson ratio	0.3	Velocity of sound in water [m/s]	1560

The load and boundary conditions that are used in the analysis are determined after material properties are assigned to the created model. Flow directions belonging to the Eulerian part are shown in Figure 2.a. Velocity profile of the Linear Wave Theory given in Eq. (1) is defined for the inlet surface. The same parameters as inlet surface are applied to far fields. On the other hand, there is no definition in the outlet surface, and parameters are determined by the software.

The meshing operation is the last step of the finite element modelling. The mesh structure of Eulerian and Lagrangian parts is presented in Figure 2.b. A 4-node doubly curved thin or thick shell, reduced integration, hourglass control, finite membrane strains elements (S4R), are used in the Lagrangian part. Besides, an 8-node linear Eulerian brick, reduced integration, hourglass control elements (EC3D8R) are utilized in Eulerian part.

The models are divided into nodes to perform and make complex analysis more simple, so as to analyse complex models in the finite elements analysis software. The distance between nodes in the Lagrangian part is 0.01 m. In the Eulerian part, the node distance is 0.50 m. Thus, the whole finite element model is made of 154446 nodes and 155456 elements in the Lagrangian part and 2073981 nodes and 2016000 elements in the Eulerian part. The equation of motion, for structure that finite elements program utilizes under external forces (F), can be written as follows.

$$m^{NJ} \ddot{X}_t^N = (F^J + I^J)_t \quad (13)$$

In Equation (13) m^{NJ} is the mass matrix, F^J is the external applied load vector transferred from the Eulerian part, I^J is the internal force vector caused by internal stresses of elements, and \ddot{X} symbolizes acceleration. I^J is obtained from individual elements such that the global stiffness matrix does not need to be formed. The coupled Eulerian-Lagrangian analyses can be performed only in dynamic, explicit steps [19]. The explicit integration rule

given in the following equations is used to obtain displacements that are transferred from structure to fluid.

$$\dot{X}_{\left(i+\frac{1}{2}\right)}^N = \ddot{X}_{\left(i-\frac{1}{2}\right)}^N + \frac{\Delta t_{(i+1)} + \Delta t_{(i)}}{2} \ddot{X}_{(i)}^N \quad (14)$$

$$X_{(i+1)}^N = X_{(i)}^N + \Delta t_{(i+1)} \dot{X}_{\left(i+\frac{1}{2}\right)}^N \quad (15)$$

X^N is a degree of freedom of the displacement component, and the subscript i is the increment number of explicit dynamic steps. The central-difference integration operator is explicit with regards to the advancement of the kinematic state according to well-known values of $\dot{X}_{\left(i-\frac{1}{2}\right)}^N$ and $\ddot{X}_{(i)}^N$ taken from the previous increment. Nodal accelerations are obtained from Equation (16) as given below.

$$\ddot{X}_{(i)}^N = (m^{NJ})^{-1} (F_i^J - I_i^J) \quad (16)$$

Iterations are not required in the mentioned method to update the displacement, velocity and acceleration values. In addition to explicit analysis, modal analyses are also performed simultaneously to obtain natural frequencies. The finite element of the model is given by the following matrices in Equation (17). The Lanczos Method is utilized to solve matrixes [19], where λ is the square of natural frequency [29].

$$[K]\{X\} - \lambda [m]\{X\} = 0 \quad (17)$$

3.2. Semi-analytical analysis

The numerical analysis and semi-analytical analysis are simultaneously maintained in this part of the study. The displacement and natural frequency values that are obtained from numerical analysis are compared by semi-analytical analysis. The structure is idealized as a lumped mass tower. Forces which affect the structure, not including the fluid model, are applied to the reduced system. The current model and application points of the forces are shown in Figure 1. Total masses in the storeys are placed as lumped masses to the corresponding points. The analysis of a two degree of freedom system under environmental forces is used in Equation (18).

$$m\ddot{X} + c\dot{X} + kX = F \quad (18)$$

Equation (18) is used to calculate the displacement and natural frequency values of the model having two degrees of freedom. The coordinate transformation is applied to Equation (18) from Equation (19), and Equation (20) is obtained in the end. The modal shape matrix $[\phi]$, determined according to structural modes, is used to coordinate transformation.

$$\{X\} = [\phi]\{\xi\} \tag{19}$$

$$[\phi]^T[M][\phi]\{\ddot{X}\} + [\phi]^T[C][\phi]\{\dot{X}\} + [\phi]^T[K][\phi]\{X\} = [\phi]^T\{F(t)\} \tag{20}$$

The equation is solved by initial conditions below, according to Runge–Kutta method to obtain point displacements.

$$\xi_{1(0)} = \xi_{2(0)} = \dot{\xi}_{1(0)} = \dot{\xi}_{2(0)} \tag{21}$$

The Runge–Kutta method, as shown below, is used to evaluate simple relationships at the beginning, in the middle, and at the end of all overall time steps (Δt) [30].

$$\begin{aligned} \ddot{X}_{(t)} &= m^{-1}(F_{(t)} - c\dot{X}_{(t)} - kX_{(t)})\dot{X}_{t+\Delta t} \\ &= \dot{X}_t + \ddot{X}_{t+\Delta t}, X_{t+\Delta t} = X_t + \dot{X}_{t+\Delta t} \end{aligned} \tag{22}$$

In addition to displacements, natural frequency of the structure (ω) is obtained by Equation (23).

$$[K] - \omega^2[m] = 0 \tag{23}$$

Natural frequency of a damped system is always lower than natural frequency for an undamped system. Besides, the frequency value decreases with an increase in damping ratio. The damped natural frequency value of the system is calculated using the damping ratio (ξ) according to Equation (24).

$$\omega_d = \omega\sqrt{1-\xi^2} \tag{24}$$

3.2.1. Application of semi-analytical analysis to template structure

The mass, damping and stiffness values of the first storey, which are used to constitute the mass, damping and rigidity matrices, are $m_1 = 55.05 \times 10^3$ kg, $c_1 = 11.65 \times 10^3$ Ns/m and $k_1 = 2060.97 \times 10^3$ N/m, respectively. In addition, the mass, damping and stiffness values for the second storey are calculated as $m_2 = 44.52 \times 10^3$ kg, $c_2 = 6.08 \times 10^3$ Ns/m and $k_2 = 519.12 \times 10^3$ N/m, respectively. The matrices of mass, damping and stiffness, as based on the determined values, are given in Eqs. (25-27). The damping coefficient (ξ) is taken to be 0.02 in this study [31].

$$m = \begin{bmatrix} 55.05 \times 10^3 & 0 \\ 0 & 44.52 \times 10^3 \end{bmatrix} \tag{25}$$

$$c = \begin{bmatrix} 17.73 \times 10^3 & -6.08 \times 10^3 \\ -6.08 \times 10^3 & 6.08 \times 10^3 \end{bmatrix} \tag{26}$$

$$k = \begin{bmatrix} 2060.97 \times 10^3 & -519.12 \times 10^3 \\ -519.12 \times 10^3 & 519.12 \times 10^3 \end{bmatrix} \tag{27}$$

In addition, the modal shape matrix is converted to the matrix form as given below.

$$\phi = \begin{bmatrix} 1 & 1 \\ 3.12 & -0.39 \end{bmatrix} \tag{28}$$

The respective total loads lumped at nodes are computed by integrating these loads over appropriate structural members. The total wave force ($F_{1(t)}$) is affected to point 1. Wave forces affecting legs, horizontal bracings, and diagonals in the first storey of the structure constitute $F_1(t)$ and are calculated one by one according to Equation (3). The wind force (F_2) affecting the model is calculated as $F_2 = 218701$ N in Equation (5) for tower at the second point. The wind and wave forces constitute external forces of the right side in the equation of motion. Eqs. (24-26) are placed into the equation of motion in Equation (13) and the equation is solved. Both semi-analytical and finite element methods are continued for 10 wave period durations, that is for 60 s, with the step interval length of (Δt) 0.01s.

4. Results

The free surface elevation, displacements, and frequency values that are obtained by different analyses are comparatively presented in this section of the study. Mode shapes and stress distributions, which are determined by the software, are also presented.

Time variations of free surface elevations for different positions are presented in Figure 3. The values obtained for two different locations, according to sizes of the numerical model, are also given in that figure.

The free surface elevation that is analytically obtained for $x = 0$ position oscillates between -2.00 and +2.00. The numerical

Table 2. Natural frequency and displacement values

Analysis	Natural frequency [rad/s]		Maximum displacement [m]	
	ω_{d1}	ω_{d2}	X_1	X_2
Numerical	2.5692	5.4821	0.3789	0.5912
Semi-analytical	2.8159	6.4146	0.4247	0.6813

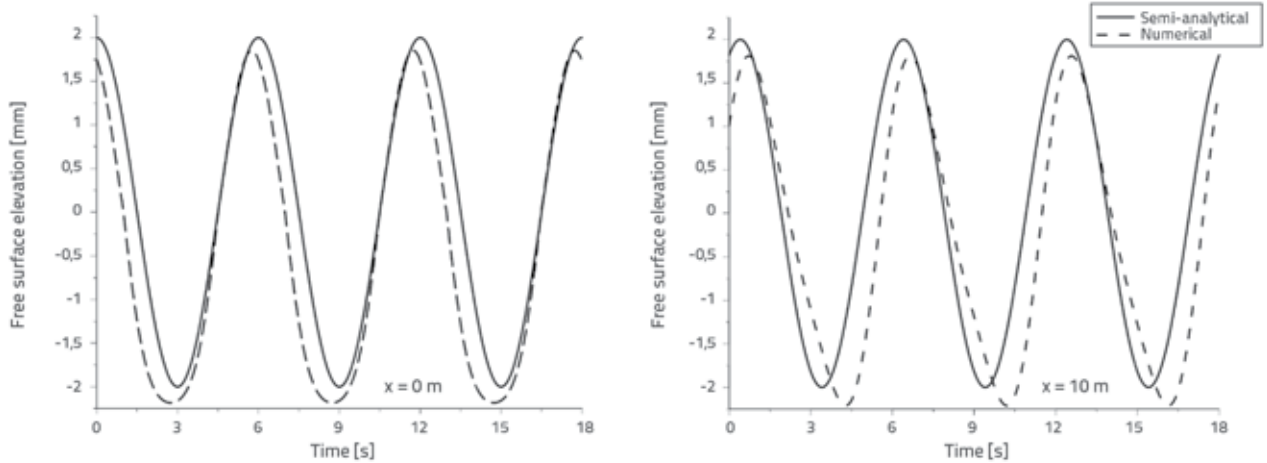


Figure 3. Free surface elevations

value for the same position ranges between -2.18 and +1.85. On the other hand, while the oscillation for $x = 60$ m position is analytically between -2.00 and +2.00, the oscillation for the same position is numerically between -2.12 and +1.81. The maximum difference between the analytical and numerical results is 9.75 %.

Mode shapes of the structure and the corresponding natural frequency values are obtained by numerical analysis. The results are given in Figure 4.

Natural frequency values that are obtained from numerical analysis are also determined using Equation (24). While the first natural frequency of the two degree of freedom system is calculated as 2.8159 rad/s, the second natural frequency value is determined as 6.4146 rad/s. It can be seen that the difference between the two types of analysis varies between 12.08 % and 15.24 %.

Natural frequency values of mode shapes are given in Table 2. Time varying displacement values given in Table 2 are shown in Figure 5. While the difference between the first point displacements is 9.68 %, the difference is 14.58 % at the

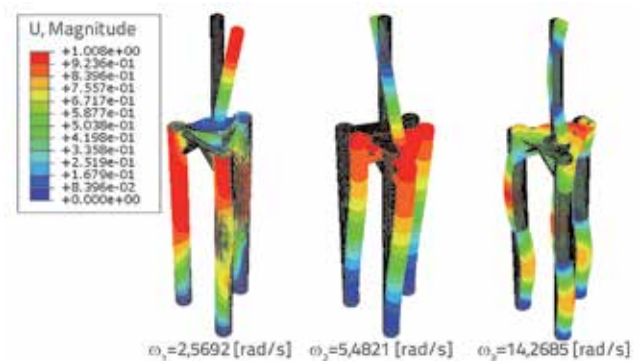


Figure 4. Mode shapes and corresponding natural frequencies of the structure

second point. The flow environment surrounding the structure, together with structural results, is also obtained. Structural displacement, which varies due to wave movement and free surface elevations of the wave for different time periods, is shown in Figure 6.

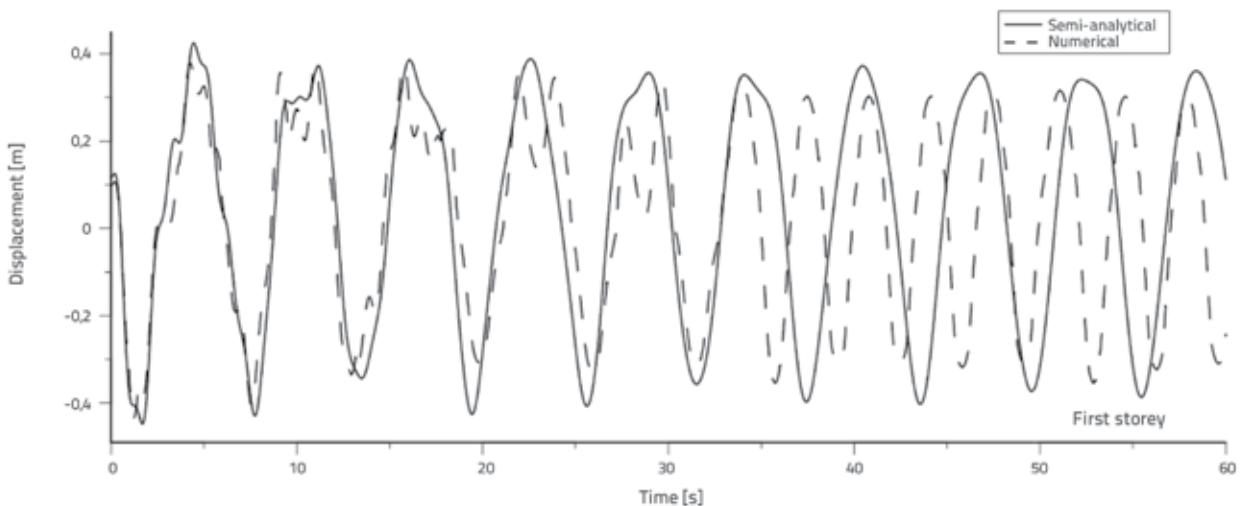


Figure 5. Time varying displacement values (first floor)

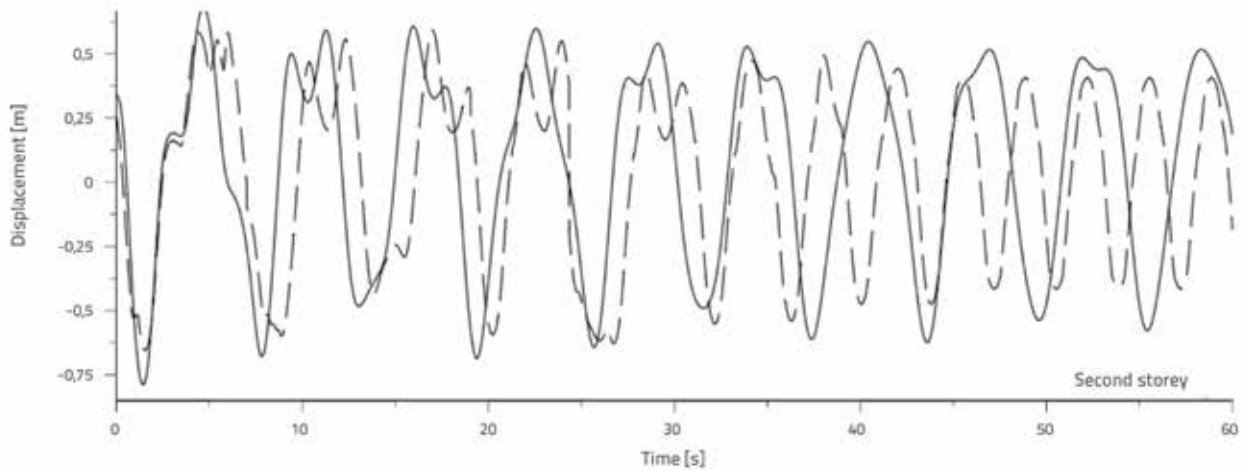


Figure 5. Time varying displacement values (second floor)

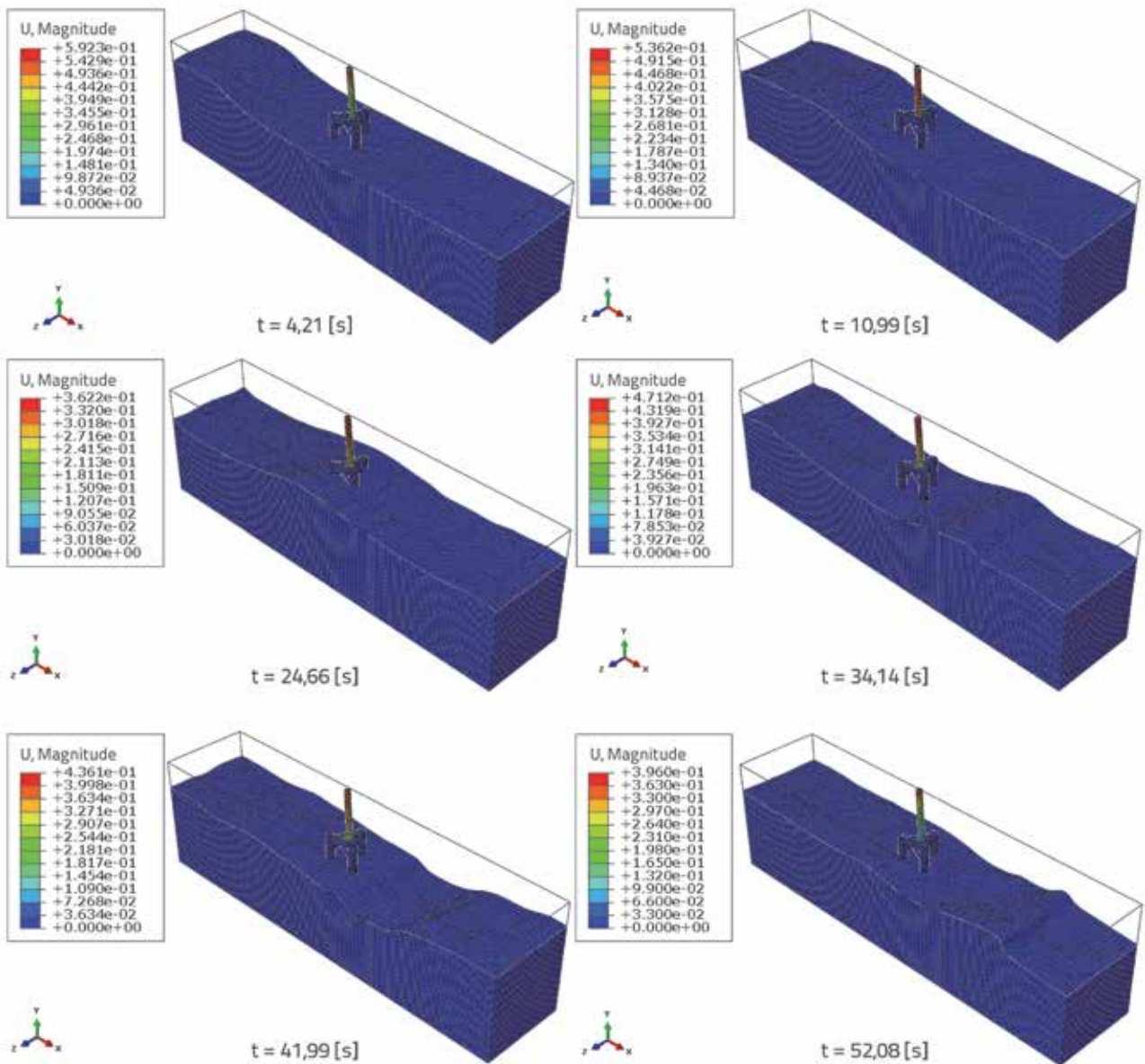


Figure 6. Coupling of fluid and structure

5. Conclusion

The fluid-structure interaction analysis of an offshore wind turbine is performed in this study by considering two different analyses. First of all, verification of the numerical model is implemented through free surface elevation. Motion of free surface elevation, modelled by CEL approach, is numerically obtained. Afterwards, the motion is analytically determined using the free surface elevation equation relating to the linear wave theory. Free surface elevation results are presented. The accordance of free surface elevations is investigated both numerically and visually. While the accordance of free surface elevations is investigated, only the wave model is constituted, without placing the structure inside. Since the flow structure deteriorates when placing the structure inside, comparison with the analytical method would not give proper results.

Natural frequency results are investigated after free surface verification. Frequency values of first two modes are obtained. Corresponding mode shapes are presented. When mode shapes are investigated, among all modes the third mode appears to be torsion one. It can be seen that natural frequency values of numerical and semi-analytical results are close to each other.

Time varying displacement values for two different analyses are shown in figures. Maximum displacement values of points are given in tables. Maximum displacement values are obtained at the peak point as expected. Time varying displacement values obtained by two different analyses are compatible with each other, and these values represent the effect of wave motion on the structure. Change in motion of the structure due to wave motion is presented. A compatible behaviour between the structure and wave period has been demonstrated.

Wave forces calculated by a finite element analysis program are transferred to the structure by CEL technique, and structural analysis is performed. The accuracy of semi-analytical and finite elements analyses results is determined in the end. Because

node and element numbers make FEM analyses more difficult when structure height increases, semi-analytical analysis can be used as an alternative method when fluid outputs are not necessary.

The CEL technique presented in this study enables determination of the fluid-structure interaction by one interface. In the case of solving the same physical problem by only Lagrangian method instead of Eulerian-Lagrangian methods, two different interfaces are required at the same time. While one of the interfaces belongs to the fluid model, the other is for structural model. Interaction of the surfaces is in such case provided by contact surfaces. Contact surfaces of solid and fluid models must be correctly defined to provide the interaction. Therefore, mesh densification is needed for the related regions. This situation also increases the required node and element numbers in the analysis. Because of this reason, various mesh sizes are considered in both Lagrangian and Eulerian parts. The results in Figure 3 show the compatibility of mesh sizes in the analyses. Contact surfaces are defined as co-simulation boundary conditions in the finite element analysis program. In this way, forces from fluid to structure and displacements of the structure to fluid are transferred separately. There is no need to define contact surfaces and interaction in CEL analyses, which are performed by a single interface. The contact is provided by defining the penalty contact.

The use of different interfaces, and increase in the number of nodes and elements, result in greater memory requirement. This situation also extends the solution-finding time. For this reason, using Eulerian-Lagrangian methods together for similar fluid-structure interaction problems may prove advantageous. In addition, it is also known that more reliable results for the interaction problems under big deformations are obtained when Eulerian-Lagrangian methods are used together. The results of this study will be useful for future studies that investigate various wave theory effects on structural behaviour.

REFERENCES

- [1] Tran, T.T., Kim, D.H.: The coupled dynamic response computation for a semi-submersible platform of floating offshore wind turbine, *Journal of Wind Engineering and Industrial Aerodynamics*, 147 (2015), pp. 104-119.
- [2] Wu, X., Hu, Y., Li, Y., Yang, J., Duan, L., Wang, T., Adcock, T., Jiang, Z., Gao, Z., Lin, Z., Borthwick, A., Liao, S.: Foundations of offshore wind turbines: A review, *Renewable Energy*, 104 (2019), pp. 379-393.
- [3] Ishihara, T., Zhang, S.: Prediction of dynamic response of semi-submersible floating offshore wind turbine using augmented Morison's equation with frequency dependent hydrodynamic coefficients, *Renewable Energy*, 131 (2019), pp. 1186-1207.
- [4] Uzunoglu, E., Soares, C.G.: A system for the hydrodynamic design of tension leg platforms of floating wind turbines, *Ocean Engineering*, 171 (2019), pp. 78-92.
- [5] Shi, W., Han, J., Kim, C., Lee, D., Shin, H., Park, H.: Feasibility study of offshore wind turbine substructures for southwest offshore wind farm project in Korea, *Renewable Energy*, 74 (2015), pp. 406-413.
- [6] Ma, H., Yang, J., Chen, L.: Effect of scour on the structural response of an offshore wind turbine supported on tripod foundation, *Applied Ocean Research*, 73 (2018), pp. 179-189.
- [7] Chella, M.A., Bihs, H., Myrhaug, D.: Wave impact pressure and kinematics due to breaking wave impingement on a monopole, *Journal of Fluids and Structures*, 86 (2019), pp. 94-123.
- [8] Lin, Y.H., Chen, J.F., Lu, P.Y.: A CFD model for simulating wave run-ups and wave loads in case of different wind turbine foundations influenced by nonlinear waves, *Ocean Engineering*, 129 (2017), pp. 428-440.

- [9] Ma, P., Liu, R., Lian, J., Zhu, B.: An investigation into the lateral loading response of shallow bucket foundations for offshore wind turbines through centrifuge modelling in sand, *Applied Ocean Research*, 87 (2019), pp.192-203.
- [10] Li, M., Zhang, H., Guan, H.: Study of offshore monopile behaviour due to ocean waves, *Ocean Engineering*, 38 (2011) 17-18, pp. 1946-1956.
- [11] Luengo, J., Negrob, V., García-Barba, J., Lopez-Gutierrez, J.S., Esteban, M.D.: New detected uncertainties in the design of foundations for offshore wind turbines, *Renewable Energy*, 131 (2019), pp. 667-677.
- [12] Lupieri, G., Contento, G.: A numerical study on the viscous effects of waves travelling past a weakly submerged cylinder, *Brodogradnja/Shipbuilding*, 67 (2017) 4, pp. 61-79.
- [13] Martínez, E.L., Quiroga, A.G., Jardini, A.L., Filho, R.M.: Computational fluid dynamics simulation of the water – sugar cane bagasse suspension in pipe with internal static mixer, *Computer Aided Chemical Engineering*, 26 (2019), pp. 683-688.
- [14] Gücüyen, E., Erdem, R.T., Gökkuş, Ü.: FSI analysis of submarine outfall, *Brodogradnja/Shipbuilding*, 67 (2016) 2, pp. 67-80.
- [15] Korobenko, A., Yan, J., Gohari, S.M.I., Sarkar, S., Bazilevs, Y.: FSI Simulation of two back-to-back wind turbines in atmospheric boundary layer flow, *Computers and Fluids*, 158 (2017), pp. 167-175.
- [16] Hao, W., Yuan-Sheng, C., Da-Ming, P., Wei-Wei, H., Lin, G.: Water entry hydroelasticity analysis of lattice sandwich panel with imperfection: simulation and engineering model, *Brodogradnja/Shipbuilding*, 70 (2019) 2, pp. 33-59.
- [17] Kreuzer, E., Solowjow, E., Qiu, G., Hamann, T., Grabe, J.: *Leg-Seabed Interactions of Jack-Up Vessels Due to Motions in Irregular Waves*, ASME 33rd International Conference on Ocean, Offshore and Arctic Engineering (OMAE), San Francisco, 2014.
- [18] Aboshio, A., Ye, J.: Numerical study of the dynamic response of inflatable offshore fender barrier structures using the Coupled Eulerian–Lagrangian discretization technique, *Ocean Engineering*, 112 (2016), pp. 265-276.
- [19] ABAQUS User's Manual, Version 6.12, SIMULIA, Dassault Systèmes Simulia Corp., 2015.
- [20] Aquelet, N., Souli, M., Olovsson, L.: Euler–Lagrange coupling with damping effects: application to slamming problems, *Computer Methods in Applied Mechanics and Engineering*, 195 (2006), pp. 110-132.
- [21] Ducobu, F., Riviere-Lorphevre, E., Filippi, E.: Application of the Coupled Eulerian-Lagrangian (CEL) method to the modelling of orthogonal cutting, *European Journal of Mechanics A/Solids*, 59 (2016), pp. 58-66.
- [22] Gücüyen, E., Erdem, R.T., Gökkuş, Ü.: Irregular wave effects on dynamic behaviour of piles, *Arabian Journal for Science and Engineering*, 38 (2013) 5, pp. 1047-1057.
- [23] Hao, E., Liu, C.: Evaluation and comparison of anti-impact performance to offshore wind turbine foundations: Monopile, tripod, and jacket, *Ocean Engineering*, 130 (2017), pp. 218-227.
- [24] Luczak, M.M., Telega, J., Zagato, N., Mucchi, E.: On the damage detection of a laboratory scale model of a tripod supporting structure by vibration-based methods, *Marine Structures*, 64 (2019), pp. 146-160.
- [25] Dyrbye, C., Hansen, S.O.: *Wind loads on structures*, John Wiley & Sons, Ltd. UK., 2004.
- [26] Benson, D.J., Okazawa, S.: Contact in a multi-material Eulerian finite element formulation, *Computer Methods in Applied Mechanics and Engineering*, 193 (2004), pp. 4277-4298.
- [27] Reddy, J.N.: *Principles of continuum mechanics*, Cambridge University Press, New York, USA, 2010.
- [28] Liu, H., Xu, K., Zhao, Y.: Numerical investigation on the penetration of gravity installed anchors by a coupled Eulerian–Lagrangian approach, *Applied Ocean Research*, 60 (2016), pp. 94-108.
- [29] Reddy, J.N.: *An Introduction to the Finite Element Analysis*, Oxford University Press, 2004.
- [30] Barltrop, N.D.P., Adams, A.J.: *Dynamics of Fixed Marine Structures*, 3rd edition, Atkins Oil and Gas Engineering Limited, 1991.
- [31] Bisoi, S., Haldar, S.: Dynamic analysis of offshore wind turbine in clay considering soil–monopile–tower interaction; *Soil Dynamics and Earthquake Engineering*, 63 (2014), pp. 19-35.